JOURNAL OF MATERIALS SCIENCE **40** (2005) 5859–5866

Finite element modeling concepts and linear analyses of 3D regular open cell structures

MATHIAS H. LUXNER*
Institute of Lightweight Design and Structural Biomechanics, Vienna University of Technology, Vienna, Austria
E-mail: luxner@ilsb.tuwien.ac.at

JUERGEN STAMPFL
Institute of Materials Science and Technology, Vienna University of Technology, Vienna, Austria

HEINZ E. PETTERMANN
Institute of Lightweight Design and Structural Biomechanics, Vienna University of Technology, Vienna, Austria

Various Finite Element modeling concepts and linear analyses of 3D regular cellular solids (lattice structures) with relative densities ranging from 10% to 20% are presented. Continuum element based models and beam element based models are employed, the latter with and without an adaptation of stiffness in the vicinity of the vertices. Space filling unit cell models are used for a constitutive characterization of four different structures in terms of density and directional dependence of their Young's moduli. Finite structure models of different size are simulated for investigating the influence of free surfaces and being compared to results of uniaxial compression tests of samples fabricated by two different Rapid Prototyping techniques.

1. Introduction

Highly porous, cellular solids form the basis of many biological and engineering structures. They gain increasing importance especially in the growing field of scaffold engineering [1]. The main advantages of cellular solids are their high specific stiffness and high specific strength as well as the possibility of tailoring their properties by designing appropriate cell architectures. The latter requires knowledge of the relationship between their architecture and their overall properties. Several analytical and numerical approaches have been developed. Analytical models based on beam theory have been derived [2] giving the effective mechanical properties as a function of the structures' relative density. Various analytical and numerical techniques considering the effective elastic behavior of low density regular cellular solids are presented in [3, 4]. Modeling approaches based on tetrakaidecahedral unit cells have been widely used for studying cellular structures. Analytical methods [5] and Finite Element simulations based on beam elements [6] are used for analyzing the effective stiffness of open cell metallic foams with tetrakaidecahedral unit cells. In [6] a comparison of numerically, analytically, and experimentally obtained results is reported. In [7] the elastic moduli and initial yield strength of hollow-sphere arrangements are analyzed using continuum element based Finite Element simulations. Analytical and numerical analysis of the effective stress-strain behavior of 2D model foams in the finite strain regime are presented in [8]. With respect to closed cell metallic foams a comprehensive treatise of simulation methods on both the micro and the macro scale can be found in [9–11].

The present study is embedded in a larger project concerned with cellular solids. The general aim is to gain knowledge about the mechanical behavior of cellular structures which are designed, fabricated by rapid prototyping, experimentally characterized [12, [13], and computationally simulated [14]. This paper deals with numerical simulations of 3D regular open cell structures by means of the Finite Element Method (FEM). Various modeling approaches are introduced to analyze four generic 3D structures. The structures are chosen to cover a wide range of different connectivities (number of vertices over number of struts), presumably leading to different deformation mechanisms. Fig. 1 shows the base cells of the investigated structures, Simple Cubic (SC), Gibson Ashby (GA), Body Centered Cubic (BCC), and Reinforced Body Centered Cubic (RBCC). The base cells have equal size, being build by struts with circular cross

*Author to whom all correspondence should be addressed.
0022-2461
DOI: 10.1007/s10853-005-5020-y

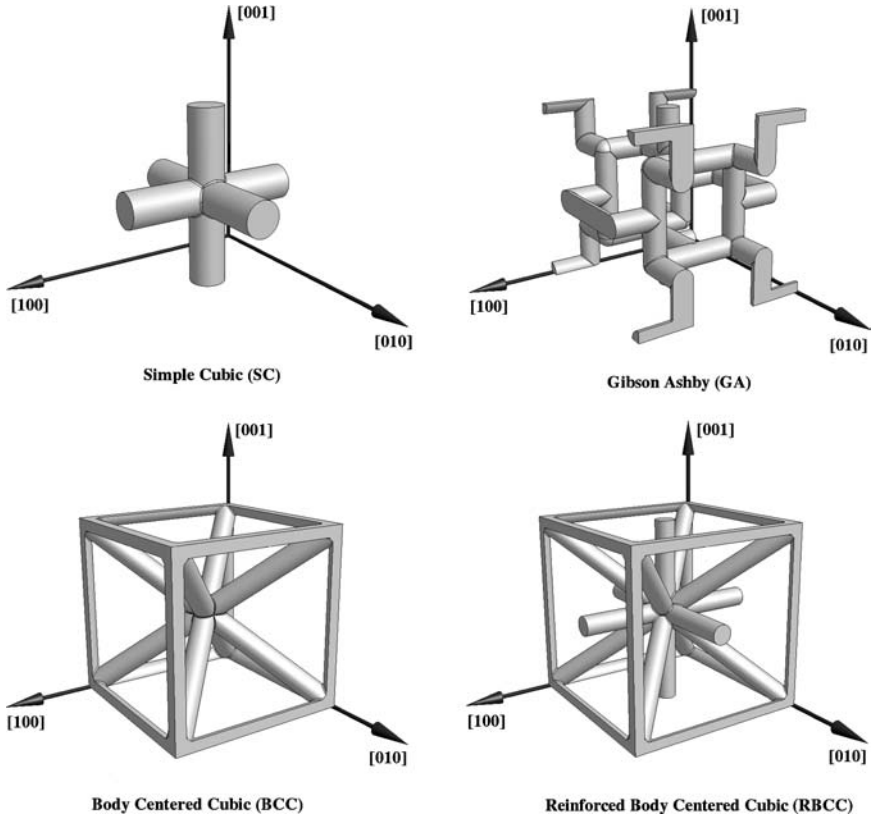

Figure 1 Base cells of the investigated structures, all of equal size and relative density of 10%.

sections. The strut diameter is constant within each individual structure. By repeating these base cells in the three principal directions periodic structures are obtained. All structures are of cubic material symmetry. The bulk material of the structures is a polymer for which isotropic, linear elastic material behavior is assumed.

Three different FEM modeling techniques are utilized and their applicability is assessed with respect to modeling cost and quality of the results. As a computationally cheap approach, higher order beam elements are used for modeling the structures. Straightforward discretization by beam elements is used as well as a beam modeling approach adapting the stiffness and the material distribution in the vicinity of the vertices. Continuum element models are employed for highly detailed analyses, being computationally much more expensive and requiring high modeling effort.

The structures are treated as infinite and finite media, employing unit cell models and finite size models, respectively. The latter are variable in size, as being composed of a given number of base cells. Differences of the modeling approaches are discussed and comparability of the respective results is evaluated.

Constitutive characterization of the 3D cellular structures for the linear elastic regime is done by determination of the entire elasticity tensors using the unit cell models from which the directional dependence of the Young's modulus is derived. The density dependence of the Young's modulus is described for varying structures and orientations.

Corresponding specimens are fabricated using two different Rapid Prototyping techniques and being tested by means of uniaxial compression. The extent of free surface effects is investigated by simulating finite samples of different size, and a comparison of computational predictions with experimental results is shown.

2. Finite element models

All numerical investigations are carried out by means of the Finite Element package ABAQUS/Standard (*Version 6.4.3, HKS, Pawtucket, RI*). In this section three different FEM modeling techniques are presented. Beam element based models are utilized for unit cell analyses and for the simulation of finite samples. For a highly detailed representation of the structures, continuum element based unit cell analyses are used. They are taken as reference models to assess the applicability of the beam element based models.

2.1. Beam element models

The beam element approaches employ 3D beam elements for modeling the structures. Timoshenko beam elements with quadratic interpolation functions are used to allow for bending and transverse shear deformations. At least four elements are used for discretization of a single strut.

Beam element models are computationally cheap, but straightforward modeling of a vertex by beam elements suffers from two approximations. First, it does not account for multiple volumes at overlapping domains. Second, such models do not account for possible constraints in the vicinity of the vertices, caused by the material aggregation in these domains. Thus, the distribution of the material in the intersections of the

struts should be considered in terms of stiffness and density.

To find the strut radius matching the desired relative density of the model the material distribution in a vertex is approximated by a sphere with a radius equal to the strut radius. The connected cylindrical struts end at the sphere's surface which leave gaps and may create overlaps. This approximation is used throughout this study for vertices connecting more than two struts. The accuracy of this approximation depends on the complexity of the vertices.

An adaptation of the stiffness in the vicinity of the vertices is introduced by using very stiff elements within a spherical domain around the vertices with a radius equal to the strut radius. The "rigid" behavior is achieved by setting the Young's modulus 1000 times higher the polymers's Young's modulus. This adaptation is considered preferable for vertices connecting four or more struts, but not for vertices connecting two or three struts.

2.2. Continuum element models

Tetrahedron elements with quadratic interpolation functions are employed for the continuum element based approach. This has the advantage that all features of the structures' geometries are captured in high detail. Unlike the beam element based models, the fillets between the struts, which emerge during the rapid prototyping process, are modeled by the continuum element approach. Furthermore, it is possible to study highly resolved stress and strain fields in the vicinity of the vertices. For all continuum element based models the element edge length is not larger than 1/6 of the strut diameter. Additional mesh refinement is done at the vertices (element edge length not larger than 1/12 of the strut diameter). The choosen discretization allows for an accurate representation of the deformation patterns. Considerable modeling effort and the high number of degrees of freedom, resulting in high computational cost, set the limit of applicability and size for the continuum element based models.

3. Structural models

In the previous section three different FEM modeling techniques have been presented. This section deals with two different approaches for representing the structures as infinite or finite media, respectively. Treating the structures as infinite media has the benefit that the mechanical behavior of the structures (except structural stability) can be described by looking only at the periodically repeating part of the structures, resulting in rather small numerical models. To achieve correspondence to the experimental setup the entire specimens are modeled as finite media, consequently, resulting in larger numerical models.

3.1. Infinite medium models

All investigated structures exhibit spatial periodicity. The mechanical behavior of a 3D infinitely repeated periodic structure can be described by modeling an appropriate space filling 3D unit cell with proper boundary conditions [15, 16]. Unit cells of different size and shape may be chosen for each structure. Here, base cells as shown in Fig. 1 are taken as representative unit cells for the simulations with continuum elements. For the beam element based models, struts which sit in periodic faces, are modeled in one of the faces only.

Homogenization via a periodic microfield approach is employed for analyzing the effective mechanical behavior of the infinite periodic arrangement under far field mechanical loads. An FEM based homogenization concept, also known as 'macroscopic degrees of freedom' (concept of masternodes), is employed, e.g. [15, 16]. Appropriate coupling of the degrees of freedom of the unit cell boundaries is applied to the FEM model to achieve spatial periodicity of the deformation field. Far field mechanical loads are applied to the masternodes. For the FEM modeling of the unit cells the beam element based approach and the continuum element based approach are used. A comparison of the various FEM modeling techniques will be presented in Section 5.

In order to characterize the structures by means of their effective mechanical properties the entire overall elasticity tensors of the structures are determined. For the most general case this can be done by applying six independent load cases to a unit cell model and assembling the overall elasticity tensors from the mechanical responses of the model. From the elasticity tensor the Young's modulus in any spatial direction can be computed.

3.2. Finite medium models

To assess the comparability of the unit cell predictions to experimentally obtained results, finite structures corresponding to test specimens (see Fig. 2) are analyzed in addition to the unit cell simulations. By these models free surface effects are captured and the load is applied in a well defined way.

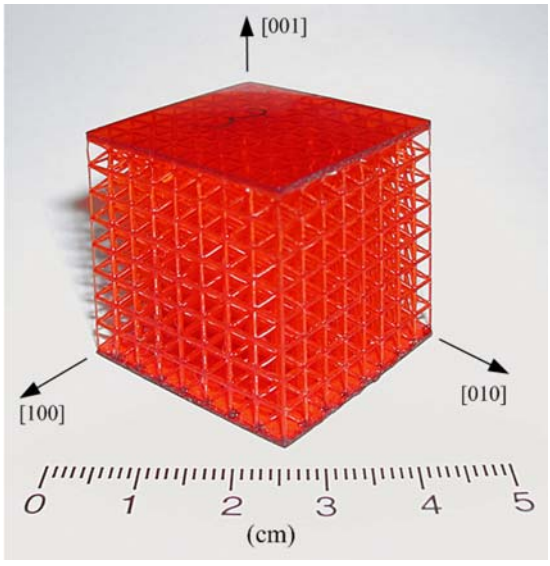

Figure 2 8×8×8 BCC test sample, fabricated by Digital Light Processing.

The top boundary conditions are chosen to represent a rigid plate, which remains parallel to the (001) plane, otherwise it can move freely, and rotate around the [001] axis. This is achieved by an appropriate coupling of the top face nodes. Furthermore, all degrees of freedom of the bottom face nodes are locked.

Beam element based FEM models are used to keep the number of degrees of freedom in a feasible range. Continuum element based FEM models of finite structures with reasonable mesh refinement are beyond computational limits.

4. Rapid prototyping and experiments

The test specimens consist of 8×8×8 base cells (see Fig. 2), with the exception of GA, which consists of 4×4×4 base cells. Bottom and top plates allow for a well-defined load application and a clear representation of the boundary conditions in the finite sample FEM models.

Two different Rapid Prototyping (RP) techniques [12] were used for the fabrication of the physical prototypes presented in this work, i.e. Digital Light Processing (DLP) and Selective Laser Sintering (SLS).

DLP is a process based on polymerization of photosensitive resins using a digital mirror device. By slicing the volume model of the cellular solids into layers of constant thickness, a series of bitmaps is generated. These bitmaps are then projected onto the resin's surface. Where the bitmap is white, the resin will solidify. Black regions of the bitmap leave the resin liquid. In contrast to traditional stereolithography [17, 18] (which uses an ultraviolet laser beam to cure the resin), DLP is based on using visible light. Therefore special resins, sensitive to visible light, have to be utilized [19].

SLS uses an infrared laser to fuse thermoplastic powder particles. By selectively scanning the surface, the outline of the object can be fused together. After one layer of the object has been completed, the build platform is coated with another powder layer and the process is repeated. The Young's modulus of the DLP material (a blend of acrylates and epoxy-based resins) was measured to be 2300 MPa, the polyamide powder used for SLS structures exhibits a Young's Modulus of 2400 MPa. The Poisson ratio for both types of materials is assumed to be 0.3.

The utilized DLP system (*Envisiontec Perfactory Mini*) allows to fabricate structures with high feature resolution (pixel size 40 μm) and good surface roughness. Minimal wall thicknesses around 0.2 mm are easily achievable. Overhanging geometries can in most cases be fabricated without using support structures. In the case of cellular materials, such support structures would be impossible to remove. SLS is able to fabricate all overhanging geometries, but regarding feature resolution (0.1 mm) and minimum wall thickness (0.4 mm) SLS is inferior to DLP. DLP as well as SLS offer reasonably high build speeds. Several samples can be built per day, thus enabling the fabrication of 4–5 samples of each geometry presented in this work.

The fabricated structures were tested using a Zwick Z250 universal testing machine. The samples were loaded in uniaxial compression, and force as well as crosshead travel were recorded. In order to allow for free movement of the samples in the plane perpendicular to the loading direction, one compression plate was floating on steel balls.

5. Results

A number of simulations and analyses are performed utilizing the modeling approaches introduced above. The results are interpreted in terms of the elastic behavior. The approaches are compared among each other as well as to experimental data.

For the unit cells, the entire elasticity tensors of the various structures are predicted in order to characterize the constitutive behavior. For the finite samples, the stiffness under uniaxial compression in various directions is simulated.

5.1. Density dependence of the Young's modulus

The relation between the density and the Young's modulus is discussed by recourse to beam element unit cell models with straightforward beam modeling. Each of the four different structures is investigated at relative densities of 10%, 12.5%, 15%, 17.5%, and 20%. The density vs. Young's modulus data are predicted for three different directions, i.e. aligned with the cubic base cell edge [001], along the surface diagonal [011], and along the cube's diagonal [111]. For each structure and in each direction the data are fitted by the exponential regression function,

$$\frac{E^*(\underline{\phi})}{E_s} = C\ {\rho_{rel}}^{\beta(\underline{\phi})}, \tag{1}$$

according to [2], where ρ_{rel} is the relative density, E_s is the Young's modulus of the bulk polymer, and $E^*(\underline{\phi})$ is the effective Young's modulus of the structure. $\beta(\underline{\phi})$ denotes the density exponent and $\underline{\phi}$ is the considered direction. The resulting density exponents are summarized in Table I. For the factor of proportionality, C, a wide scatter between 0.1 and 0.6 is found. Analyzing the many different influences on that factor is beyond the scope of this study. However, the validity of the exponent data holds, and will be discussed in the following.

It is well known, that the value of the density exponent depends on the governing deformation mechanisms in the considered directions [2, 3, 12]. For structures and loading directions, where the local deformation of the struts is stretching or shearing, the

TABLE I Density exponent for different structures and different directions in the relative density range between 10% and 20%

Structure	[001]	[011]	[111]
SC	1.00	1.83	1.85
GA	1.98	1.74	1.76
BCC	1.03	1.02	1.01
RBCC	1.01	1.02	1.02

Young's modulus changes linearly with the density. On the other hand, the Young's modulus changes with the second power of the relative density for structures and loading directions with bending dominated strut deformation [3]. From the present results in Table I it is obvious that the governing deformation mechanism for SC changes with direction. In the principal directions stretching is the prevailing deformation mechanism, because struts continuously pass through in these directions. For the [011] and [111] direction the density exponent increases, indicating a deformation mechanism dominated by strut bending.

For GA the density exponent is nearly two in the principal directions, reflecting the fact that in these directions the structure is bending dominated. The density exponent decreases for the [011] and [111] directions to 1.74 and 1.76, respectively. Thus, bending is the dominant but not the exclusive deformation mechanism in these directions.

BCC and the RBCC exhibit a density exponent close to one for the directions shown. Stretching is the principal mechanism, as a consequence of the diagonal struts oriented in favor.

5.2. Directional dependence of the Young's modulus

The directional dependence of the Young's moduli of the structures is derived from the elasticity tensors of the continuum element based unit cells. This is done for structures with a relative density of 10%. Figs 3 and 4 show the directional dependence of the Young's moduli, E^*, normalized by the Young's modulus, E_s, of the bulk material in the (100) and $(1\bar{1}0)$ plane, respectively.

SC exhibits high stiffness in the principal directions governed by axial strut loading. For deviations from the principal directions bending deformation of the struts is initiated. The latter mode gives rise to a much more compliant behavior and the normalized Young's modulus decreases rapidly.

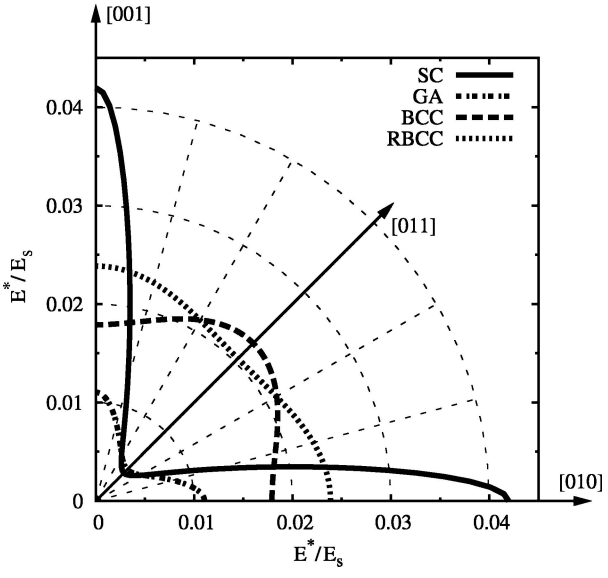

Figure 3 Comparison of the normalized Young's modulus in the (100) plane for all structures with a relative density of 10%.

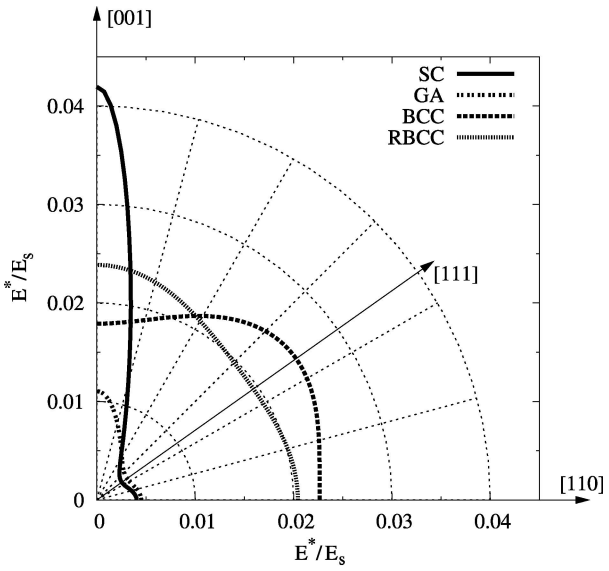

Figure 4 Comparison of the normalized Young's modulus in the $(1\bar{1}0)$ plane for all structures with a relative density of 10%.

For the bending dominated GA the principal directions are the stiffest directions, too. Deviations from the principal directions give rise to deformations of additional struts (the ones aligned with the cube's edges) resulting in lower stiffness. For almost all directions the normalized Young's modulus is much lower compared to the other structures.

Different behavior is shown by BCC, where the stiffest direction of this structure is the [111] direction. For RBCC the direction dependence of the normalized Young's modulus is less pronounced than for all other investigated structures. The directions with the highest value for the normalized Young's modulus are the principal directions. For both structures the more uniform spatial orientation distribution of the struts results in less anisotropy. Such more uniform 3D networks carry loads rather by axial strut forces and prevent local strut bending, as discussed in the previous section.

5.3. Comparison of FEM modeling techniques

The presented FEM modeling techniques are compared by means of the normalized Young's moduli for several directions of the investigated structures at 10% relative density. Figs 5 to 7 show the normalized Young's moduli in the (100) plane predicted by the following approaches; continuum element based unit cell models (dashed bold lines), beam element based unit cell models with (solid thin lines) and without (dashed thin lines) stiffness adaptation, as well as beam element based finite structure models with (open symbols) and without (filled symbols) stiffness adaptation in the vicinity of the vertices. The approximation of the density is done for all beam element based models.

The modeling of the density and the adapation of the vertex stiffness, is of approximative character. A unique treatment has been chosen for evaluating that

approach and to learn about its effect on various structural architectures. Two effects on the elastic behavior are involved, being more or less pronounced at different situations. First, the density approximation yields some gaps and/or overlaps, and, consequently, a few percent error for the strut diameter at fixed density. Second, the stiffness of the vertex tends to be overestimated for some local loading scenarios, like stretching in direction of the strut axis. It was not attempted to find a best fit for each individual structure (and maybe each loading direction and density), but rather to gain general knowledge from such an approach.

Considering both unit cell models for SC (Fig. 5) it can be seen that the stiffness in the principal directions

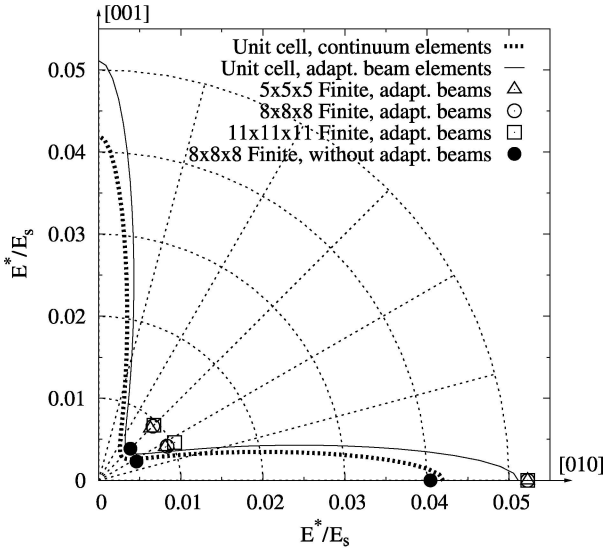

Figure 5 Comparison of modeling approaches in terms of the normalized Young's modulus in the (100) plane for SC with a relative density of 10%.

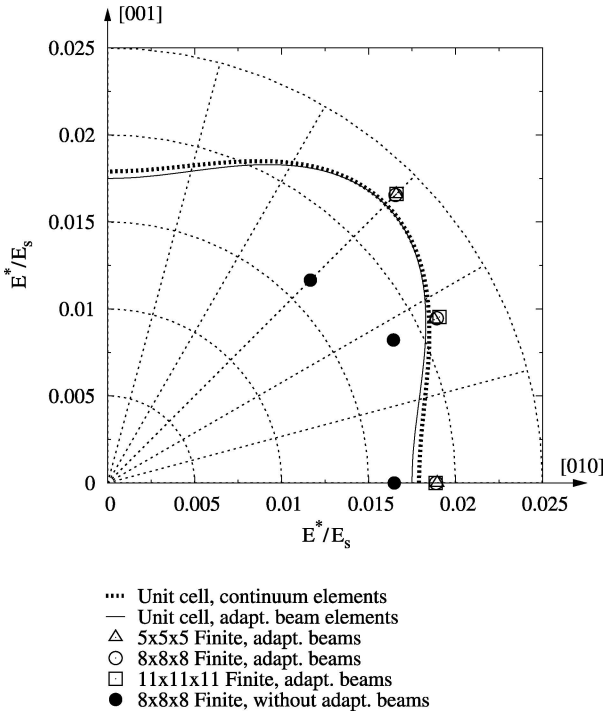

Figure 6 Comparison of modeling approaches in terms of the normalized Young's modulus in the (100) plane for BCC with a relative density of 10%.

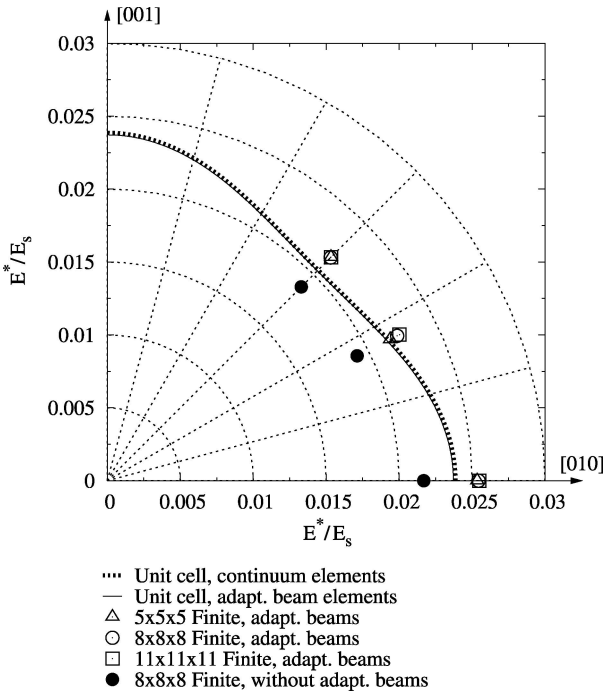

Figure 7 Comparison of modeling approaches in terms of the normalized Young's modulus in the (100) plane for RBCC with a relative density of 10%.

is overpredicted by the beam element model. This is caused by the rigid domains of the straight through struts in these directions. Deviating from the principal directions, the differences of the stiffness predictions decrease. For BCC (Fig. 6) and RBCC (Fig. 7) the stiffness predictions by the unit cell models coincide.

In contrast to the structures discussed before, beam unit cells without an adaptation of stiffness are compared to the continuum unit cells for GA, since this structure exhibits only vertices connecting three struts. Due to the high number of vertices in this structure a minor stiffening effect due to material aggregation in the vertices is neglected. On the other hand, stiffness adaptation leads to an pronounced overstiffened behavior of the beam element unit cell. This fact is shown in terms of the finite samples with applied stiffness adaptation, Fig. 8 (open symbols). In Fig. 8 it can be seen that the beam element unit cell reacts more compliant than the continuum element based unit cell model, indicating that the stiffness of the vertices is underestimated. The high number of vertices and short struts lead to less accuracy of the density approximation, also. The estimated strut radius is too large, increasing the stiffness of the structure and compensating partly for the omitted stiffness adaptation of the vertices.

The beam element models with and without adaptation of the stiffness at the vertices are compared in terms of the 8×8×8 finite structure models. In Figs 5 to 7 (open and filled circles) the values of the normalized Young's moduli for three different directions are shown. It can be seen that the finite structure models without rigid domains react less stiffly. The deviation between the two beam element models depends strongly on the topology of the structure and the governing deformation mechanism, respectively. For directions in which bending is the governing mechanism,

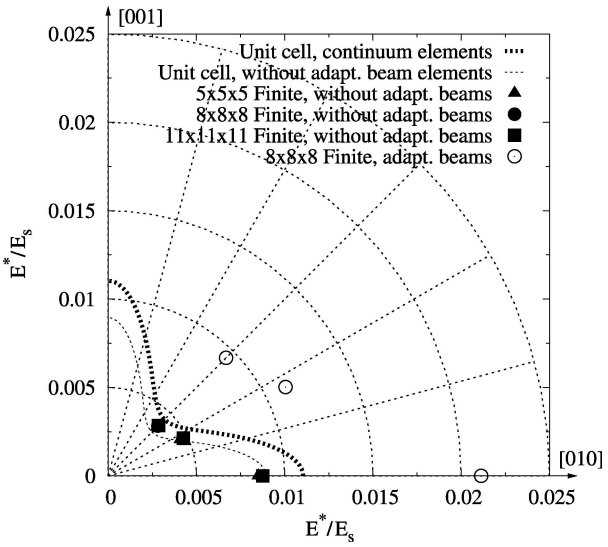

Figure 8 Comparison of modeling approaches in terms of the normalized young's modulus in the (100) plane for GA with a relative density of 10%. Note that the predictions for the finite samples without rigid beams are almost identical.

like [011] of SC, [011] of BCC, and all directions of GA the deviation is higher than for stretching dominated directions.

5.4. Influence of the specimen size

Finite samples consisting of different numbers of base cells are modeled by beam elements with adaptation of stiffness. The results are compared to the continuum unit cell models in order to assess the required testing specimen size, i.e. the effect of the free faces as well as the effect of the top and bottom plates. The latter introduce additional constraints giving rise to higher stiffness, the first ones result in a decrease of the stiffness.

Evaluation is done for three directions by means of the normalized Young's modulus. Finite samples consisting of $5\times5\times5$, $8\times8\times8$, and $11\times11\times11$ base cells are analyzed. Figs 5 to 7 show a comparison of the simulation results of the various finite sample sizes for the different structures.

It can be seen that the results of the various samples sizes correspond well for all structures. General rules, however, regarding the size of testing specimens and for extrapolation to properties of infinite structures cannot be derived from these investigations, since the surface effects strongly depend on the structure's architecture and on the governing deformation mechanisms in the considered direction.

It is noted, that the inclined direction is chosen as [021] leaving sample surfaces with minimum amount of dissected base cells. Arbitrary inclinations are expected to give rise to a more pronounced influence of the surfaces.

5.5. Comparison to experimental results

Fig. 9 shows the results of the continuum element based unit cells and the $8\times8\times8$ finite structural models with

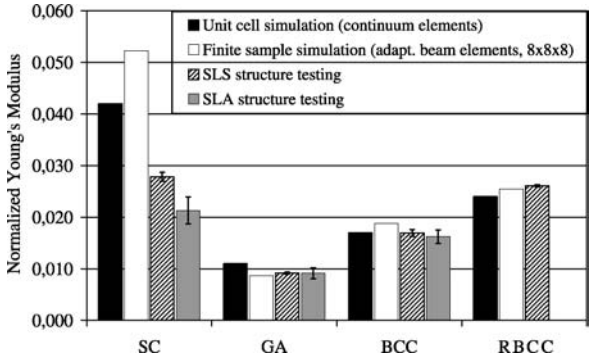

Figure 9 Comparison of experimental and simulation results regarding uniaxial compression in one of the principal directions, relative density of the structures is 10%.

stiffness adaptation in comparison to experimental results in one of the principal directions [12].

For structures with directionally less sensitive behavior such as BCC, RBCC, and GA the results correspond very well, whereas for structures with high directional sensitivity such as SC deviation of the simulation results is noticeable. For SC the geometric imperfections that occur during the fabrication process may play a significant role, as do experimental conditions. As can be seen in Figs 3 and 4 small changes in direction lead to a pronounced decrease of the normalized Young's modulus. In addition, geometrical perturbations are also expected to reduce the stiffness in the principal directions.

6. Conclusions

Various Finite Element modeling concepts and linear analyses of regular open cell structures are presented.

Continuum element based unit cell models are utilized as reference models to discuss the applicability of beam element based models with and without an adaptation of stiffness in the vicinity of the vertices. The accuracy of the beam element models' results is found to be dependent on the structures' geometries and on the governing deformation mechanisms, respectively. The mechanical behavior of all structures is represented very well by the beam models, which are shown to be suitable for modeling such structures.

Unit cell models are employed for a constitutive characterization of four different structures in terms of density and directional dependence of their normalized Young's moduli. The governing deformation mechanisms are identified. Both the mechanical properties and the deformation behavior are found to be strongly dependent on the structure's architecture, as well as on the loading scenario.

Finite samples consisting of different numbers of base cells are simulated to investigate the influence of free surfaces and load introduction. Both influences strongly depend on the structures architecture and on the sample orientation, so that no general rule regarding the specimen size can be derived from these results.

The results of the simulations are compared to experimental results by means of uniaxial compression tests. It is shown that for structures with rather high directional sensitivity imperfections play a significant role

and the results deviate. For all other structures the simulation results agree very well with the experimental results.

Acknowledgement

This work was financially supported by the Austrian Science Fund under contract P15852. The authors would like to thank Thomas Daxner, Alexander Woesz, and Peter Fratzl for many useful suggestions, comments, and discussions.

References

1 W. SUN, A. DARLING, B. STARLY and J. NAM, *Biotechnol. Appl. Biochem.* (2004) 39.
2 L. GIBSON and M. ASHBY, "Cellular Solids: Structure and Properties," 2nd ed. (Cambridge University Press, 1997).
3 J. GRENESTEDT, *Int. J. Sol. Struct.* (1999) 36.
4 R. CHRISTENSEN, *ibid.* (2000) 37.
5 H. ZHU, J. KNOTT and N. MILLS, *J. Mech. Phys. Solids* (1997) 45.
6 Y. KWON, R. COOKE and C. PARK, *J. Mat. Sci. and Eng.* (2003) A343.
7 W. SANDERS and L. GIBSON, *ibid.* (2003) A352.
8 J. HOHE and W. BECKER, *Comput. Mat. Sci.* (2003) 28.
9 T. DAXNER, H. J. BÖHM and F. G. RAMMERSTORFER, in "Metal Foams and Porous Metal Structures," edited by J. Banhart, M. F. Ashby and N. A. Fleck (Verlag MIT, Bremen, 1999) p. 283.
10 T. DAXNER, R. DENZER, H. J. BÖHM, F. G. RAMMERSTORFER and M. MAIER, *Mater.-Wiss. u. Werkst.-Techn.* (2000) 31.
11 T. DAXNER, "Multi-Scale Modeling and Simulation of Metallic Foams," Fortschritts-Berichte VDI, Reihe 18, No. 285 (VDI Verlag, Düsseldorf, 2003).
12 J. STAMPFL, M. SEYR, M. H. LUXNER, H. E. PETTERMANN, A. WOESZ and P. FRATZL, in Proceedings of 2004 MRS Spring Meeting – Biological and Bioinspired Materials and Devices, edited by J. Aizenberg, C. Orme, W. Landis and R. Wang, (2004) vol. 823.
13 A. WOESZ, J. STAMPFL and P. FRATZL, *Advanced Eng. Mat.* (2004) 6.
14 M. H. LUXNER, J. STAMPFL and H. E. PETTERMANN, in Proceedings of 2004 ASME International Mechanical Engineering Congress (ASME, New York, 2004).
15 H. BÖHM, "Mechanics of Microstructured Materials" (Springer Verlag, Wien, 2004).
16 A. ANTHOINE, *Int. J. Sol. Struct.* **2** (1995) 32.
17 P. JACOBS, "Rapid Prototyping and Manufacturing" (Society of Manufacturing Engineers, Dearborn, 1992).
18 A. GEBHARDT, "Rapid Prototyping – Werkzeuge für die schnelle Produktentwicklung" second edition (Hanser Fachbuch, München, 2000).
19 R. LISKA, F. SCHWAGER, A. WOESZ, A. PISAIPAN, S. SEIDLER and J. STAMPFL, in Proceedings Radtech 2003, Berlin (2003) p. 93.

Received December 2004
and accepted April 2005